Electronic Supplementary Material (ESI) for Inorganic Chemistry Frontiers.

Three-photon absorption iridium(III) photosensitizers featuring aggregation induced emission

Xin Lu[‡a], Chaoya Xiong[‡b], Bo Li[‡c], Wenli Du[a], Shengli Li[a], Dandan Li[c], Wen Ma[a], Xiaohe Tian[d], Qiong Zhang[a,e*] and Yupeng Tian[a,e]

[a] *College of Chemistry and Chemical Engineering, Key Laboratory of Functional Inorganic Materials Chemistry of Anhui Province, Anhui Province Key Laboratory of Chemistry for Inorganic/Organic Hybrid Functionalized Materials, Key Laboratory of Structure and Functional Regulation of Hybrid Materials (Anhui University) Ministry of Education, Institutes of Physical Science and Information Technology, Anhui University, Hefei, 230601, P.R. China. Institutes of Physics Science and Information Technology, Anhui University, Hefei 230601, China.*

[b] *School of Life Science, Anhui University, Hefei 230601, P.R. China.*

[c] *Institutes of Physical Science and Information Technology, Anhui University, Hefei 230601, P.R. China.*

[d] *Huaxi MR Research Centre (HMRRC), Functional and Molecular Imaging Key Laboratory of Sichuan Province, Department of Radiology and and National Clinical Research Center for Geriatrics, West China Hospital of Sichuan University, Chengdu, 610000, China.*

[e] *State Key Laboratory of Coordination Chemistry, Nanjing University, P.R. China.*

‡These authors contributed equally to this work.

*Corresponding author: zhangqiong.314@163.com

Table of contents

Experimental and methods

Materials and apparatus

The general chemicals were obtained from Macklin (China). Annexin V-FITC/PI Apoptosis Detection Kit were obtained from Shanghai Bestbio (China). The ^{1}H NMR spectra were recorded on at 25 °C, using Bruker 400/600 Ultra shield spectrometer were reported as parts per million (ppm) from TMS (δ). Mass Spectrometer was recorded using LTQ Orbitrap XL and Bruker Autoflex III TOF/TOF. UV-*vis* absorption spectra were recorded on a UV-265 spectrophotometer. SEM were detected by REGULUS8230*. Fluorescence measurements were carried out on a Hitachi F-7000 fluorescence spectrophotometer. Quantum yield was determined by FLUORMAX-4P. One-photon confocal microscopy imaging was acquired with a Leica SP8 confocal microscopy and 100/63 × oil-immersion objective lens. Two-photon imaging data acquisition and processing were performed using Lecia TCS SP8 DIVE FALCON which equipped with one photon excitation source and femtosecond laser (680-1080 nm, 80 MHz, 140 fs), respectively. The femtosecond laser was purchased from Chameleon UltraII. In vivo fluorescence imaging was conducted on IVIS Lumin2 III.

Lippert-Mataga

The Lippert-Mataga equation was used to evaluate the dipole moment changes of the dyes with photoexcitation. [r7, r8] The equation is shown as follows:

$$\Delta\nu = \frac{2\Delta f}{4\pi\varepsilon_0 \hbar c a^3}(\mu_e - \mu_g)^2 + b$$

$$\Delta f = \frac{\varepsilon - 1}{2\varepsilon + 1} - \frac{n^2 - 1}{2n^2 + 1}$$

❒ν is the Stokes shift (ν_{abs} - ν_{em}), ν_{abs} and ν_{em} are absorption and emission (cm^{-1}), $\hbar$ is Planck's constant, c is the speed of light in vacuum, α is the Onsager radius, b is a constant. ❒f is the orientation polarizability, μ_e and μ_g are the dipole moments of the emissive and ground states, ε_0 stands for the permittivity of the vacuum.

Two-photon excited fluorescence (2PEF) spectroscopy and two-photon absorption (2PA) cross-section

2PEF spectra were obtained by the two-photon excited fluorescence (2PEF) method with a femtosecond laser pulse and a Ti: sapphire system (680-1080 nm, 80 MHz, 140 fs) as the light source. The reference sample is Rhodamine B with a concentration of 1.0×10^{-3} M in ethanol. The concentration of **Ir-H**, **Ir-8C**, and **Ir-O** was 1.0×10^{-3} M. 2PA cross-section was calculated by using the following equation:

$$\delta = \delta_{ref} \frac{\Phi_{ref}}{\Phi} \frac{c_{ref}}{c} \frac{n_{ref}}{n} \frac{F}{F_{ref}}$$

Here, ref stand for reference sample, δ is the two-photon absorption cross section, Φ is quantum yield, c is the concentration of the sample, n is refractive index, F is two-photon fluorescence integral area. The absolute value of the two-photon absorption cross-section of the reference sample is derived from the literature. [1]

Three-photon excited fluorescence (3PEF) spectroscopy and three-photon absorption (3PA) cross-section

3PEF spectra were obtained by the multi-photon excited fluorescence method with Coherent Astrella+TOPAS Prime (1200-2600 nm, 1 kHz, 120 fs) as the light source. The reference sample is Rhodamine 6G (1.0×10^{-3} M). The concentration of **Ir-H**, **Ir-8C**, and **Ir-O** was 1.0×10^{-3} M. The multi-photon absorption cross-section were calculated by using the following equation:

$$\sigma = \frac{\gamma}{N_A \times d_0 \times 10^{-3}} \bullet \left(\frac{hc}{\lambda} \right)^2$$

Here, γ is three photon absorption coefficients, λ is wavelength of incident light, N_A is the Avogadro constant, d_0 is the concentration of the sample (1.0×10^{-3} M).

Computational details

To further study the structure-property relationship, optimization was performed on B3LYP [LANL2DZ] without any symmetry restraints and the calculations were conducted with TD-DFT {B3LYP[LANL2DZ]} method with the optimized structure. All calculations were performed using the G09 software. The singlet-singlet excitation

energies were carried out with a basis set composed of 6-31G(d, p) for C N O H atoms, and the LANL2DZ basis set for Ir atoms.

ROS-generation detection

DCFH-DA was used as the ROS-monitoring agent. 20 μL of DCFH-DA stock solution (1.0 mM) and 10 μL of **Ir-H**, **Ir-8C**, and **Ir-O** (1.0×10^{-3} M) were added to 2 mL PBS solution, and LED light (400-700 nm, 40 mW/cm^2) was employed as the light source. The emission of DCFH-DA at 525 nm was recorded under various irradiation times. [2]

Electron paramagnetic resonance (EPR) assay

EPR was used to assess the generation of $^1O_2$ by **Ir-H**, **Ir-8C**, and **Ir-O**. The spin traps 2,2,6,6-tetramethylpiperidine (TEMP for trapping $^1O_2$, 20 μL) was used to verify the species of reactive oxygen species generated by **Ir-H**, **Ir-8C**, and **Ir-O** (1.0×10^{-5} M). The EPR signals of the **Ir-H**, **Ir-8C**, and **Ir-O** (1.0×10^{-5} M) before and after LED light (400-700 nm, 40 mW/cm^2) irradiation were recorded. [3]

Singlet oxygen ($^1O_2$) generation detection

The singlet oxygen was measured by a singlet oxygen indicator named 9,10-Anthracenediyl-bis(methylene)dimalonic acid (ABDA). Briefly, 2 mL of DI water solution was mixed with **Ir-H**, **Ir-8C**, and **Ir-O** (1.0×10^{-5} M) and ABDA (100 μM). Then the cuvette was exposed to LED light (400-700 nm, 40 mW/cm^2) irradiation for different time. The absorption spectra of ABDA at 378 nm showed a gradual decline under the irradiation.

We have calculated the singlet oxygen quantum yield of **Ir-H** in DMSO solution and H_2O/DMSO mixture using Rose Bengal (RB) (Φ_{RB} = 0.75 in H_2O) as the standard according to the following equation.

$$\Phi_{PS} = \Phi_{RB} \frac{K_{PS} A_{RB}}{K_{RB} A_{PS}}$$

Here, where K_{PS} and K_{RB} are the decomposition rate constants of ABDA by the photosensitizers and RB, respectively. K_{PS} and K_{RB} represent the light absorbance by the photosensitizers and RB, respectively, which are calculated by integration of the areas under the absorption bands in wavelength range of 400-700 nm.

Cell culture

The Hep G2 cells were cultured in 25 cm^2 culture flasks in DMEM, supplemented with fetal bovine serum (10%), penicillin (100 units/mL) and streptomycin (50 units/mL) at 37 °C in a CO_2 incubator (95% relative humidity, 5% CO_2). Cells were seeded in 35 mm glass bottom cell culture dishes, at a density of 1×10^5 cells and the cells could grow when the cells reached more than 60% confluence.

Cytotoxicity assays in cells

The study of the effect of **Ir-H** on viability of cells was carried out using the methylthiazolyldiphenyl-tetrazolium bromide (MTT) assay. **Ir-H** and **Ir-8C** stock solutions were diluted by fresh medium in to desired concentration (0, 0.5, 1, 2, 4, 8, 16 μM). Cells were cultured in a 96-well plate for 24 h before experiments. The cell medium was then exchanged by different concentrations of **Ir-H** and **Ir-8C** medium solutions. They were incubated at 37 °C in 5% CO_2 for 12 h before cell viability was measured by the MTT assay. The cell medium solutions were exchanged by 100 μL of fresh medium, followed by the addition of 20 μL (5 mg/mL) MTT solution to each well. The cell plates were then incubated at 37 °C in 5% CO_2 for 4 h. After MTT medium removal, the formazan crystals were dissolved in DMSO (100 μL/well) and the absorbance was measured at 490 nm using a microplate reader. And duplicated experiments have been tested.

Furthermore, the apoptosis assay of Hep G2 cells was assessed by flow cytometry. Hep G2 cells were incubated with **Ir-H** (2 μM) for 5 min. For the PDT group, the Hep G2 cells were irradiated with a LED light (400-700 nm, 40 mW/cm^2) for 0, 5 and 15 min, respectively. For the dark group, the cells were always incubated under dark condition. Then, the cells were harvested and stained with Annexin V-FITC and PI for 30 min, then washed with PBS solution and analyzed by flow cytometry.

Cell Co-localization Assays

For co-localization experiments, Hep G2 cells are incubated with **Ir-H** and **Ir-8C** (2 μM) for 5 min. Then, the cells are treated with endoplasmic reticulum-tracker blue and lysosome-tracker blue (1 μM) for 20 min. At last, samples are washed three times by PBS solution (3 × 1 mL per well) and 1 mL of PBS solution is added into each well.

The fluorescent images of the cells are collected by confocal laser scanning microscopy. The colocalization coefficient and mean fluorescence intensity of the images are determined by the software with image J. [4]

Reactive oxygen species generation under two-photon laser in vitro

The reactive oxygen species production in living cells was also assessed. Hep G2 cells were incubated with **Ir-H** (2 μM) for 5 min. Then, the cells were washed with PBS solution and incubated with SOSG (5 μM) for 15 min, after which the cells were incubated shielded from laser or irradiated for 2, 5 min (820 nm laser, 100 mW/cm^2). And then the cells were observed by confocal laser scanning microscopy.

Annexin V-FITC and PI assay

Hep G2, 4T1 and Hela cells are incubated with **Ir-H** (2 μM) for 5 min at 35 °C with 5% CO_2, Then, the cells are further stained with Annexin V-FITC (5 μM) and PI (5 μM). and then irradiated by light (820 nm, 100 mW/cm^2) for 5 min. The fluorescent images of the cells are collected by confocal laser scanning microscopy.

Live/Dead assay with calcein AM/PI

Hep G2, 4T1 and Hela cells with a density of 10^5 cells were incubated with **Ir-H** (2 M) for 5 min. Calcein AM and PI were used to confirm the viability of Hep G2, 4T1, Hela and QSG cell lines. Fluorescence images were collected by confocal laser scanning microscopy after laser irradiation. [5]

The one/two-photon fluorescence imaging depth study

A Lecia TCS SP8 DIVE FALCON which equipped with single-wavelength laser (output wavelength: 405 nm, 458 nm, 488 nm, 514 nm, 561 nm, 633 nm) and femtosecond laser (adjustable output wavelength: 680-1080 nm, 80 MHz, 140 fs) was employed to achieve one/two-photon fluorescence imaging. Hep G2 cells were treated with **Ir-H** (2 μM). And then, slices were prepared from cardiac muscle tissue in Balb/c mice. The tissue sections were cut to 100 mm thickness. The tissue section was incubated with **Ir-H** (2 μM) for 30 min. The one-photon fluorescence emission was observed from 650 ± 20 nm upon excitation at 405 nm (0.5 W/cm^2). The two-photon fluorescence emission was observed from 600 ± 20 nm upon excitation at 820 nm (0.5 W/cm^2). [6]

Animal experiments

All the animal procedures were approved by the Institutional Animal Care and Use Committee of Anhui University (serial number: 2021-042) based on the National Standard of China GB/T35892-2018 guidelines for Ethical Review of Experimental Animal Welfare. We have taken great efforts to reduce the number of animals used in these studies and also taken effort to reduce animal suffering from pain and discomfort. Female nude mouse was subcutaneously injected with 0.1 mL cell suspension containing 5×10^5 Hep G2 cells. When the tumor size was 50-100 mm^3, the mice was treated via intratumorally injection with **Ir-H** (1 mM, 20 μL). Mice were anesthetized by inhalation with a mixture of isoflurane and oxygen, fluorescence imaging measurements were conducted after 1 h, 2 h, 8 h and 24 h, respectively on IVIS Lumin2 III. The mouse was then dissected after injecting for 24 h to get organs of lung, kidney and tumor and conduct imaging on IVIS Lumin2 III.

Abbreviations

Full name	Abbreviation	Full name	Abbreviation
dimethyl sulfoxide	DMSO	water	H_2O
singlet oxygen	$^1O_2$	water fraction	f_w
Fluorescein isothiocyanate	FITC	Propidium iodide	PI
Acetylmethoxy methyl	AM	2,7-dichlorodihydrouorescein diacetate	DCFH-DA
9,10-anthracenediyl-bis(methylene)dimalonic acid	ABDA	singlet oxygen sensor green	SOSG

Synthesis of L

Ammonium acetate (7.70 g, 0.10 mol), ethyl vanillin aldehyde (1.50 g, 0.01 mol) and 1-tetrahydronaphthalone (3.00 g, 0.02mol) were added into a round-bottom flask, then added 25 mL glacial acetic acid as solvent, the solution was stirred at room

temperature until the reactants were completely dissolved, and then reacted at 100 °C for 10 hours. After the end of the reaction, black oil is obtained, and a large amount of ethanol was added to disperse it to beige solid. Yield: 87%. ^{1}H NMR (400 MHz, d_6-DMSO, room temperature) δ 9.12 (s, 1H), 8.42 (d, J = 7.6 Hz, 2H), 7.39 (t, J = 7.5 Hz, 2H), 7.32 (t, J = 7.3 Hz, 2H), 7.25 (d, J = 7.4 Hz, 2H), 6.93 (d, J = 7.9 Hz, 1H), 6.81 (s, 1H), 6.66 (d, J = 8.0 Hz, 1H), 4.02 (q, J = 6.9 Hz, 2H), 2.80 (t, J = 7.0 Hz, 4H), 2.71 – 2.59 (m, 4H), 1.32 (t, J = 6.9 Hz, 3H). ^{13}C NMR (100 MHz, d_6-DMSO, room temperature) δ 149.7, 149.0, 148.7, 138.2, 135.3, 129.6, 129.2, 128.1, 127.3, 125.2, 121.6, 116.1, 114.5, 64.4, 27.8, 25.8, 15.2. ESI-MS m/z: calcd for 419.1885, found 420.1958 ($[M+H]^+$).

Synthesis of L-O

L (2.4 g, 5.7 mmol) was dissolved in 30 mL acetonitrile, K_2CO_3 was added after L was completely dissolved and added (0.69 g, 5 mmol) with a catalytic amount (0.02 g) of 18-corone-6 (crushed). After stirring for 30 min with oil seal, 1-((2-(2-methoxyethoxy)ethyl)sulfonyl)-4-methylbenzene (1.65 g, 6 mmol) was added, and the reaction lasted for 12 h. After cooling to room temperature, slightly buttery substance was got through filtering and washing with acetonitrile. The white product **L-O** (3.1 g) was obtained by recrystallization with ethanol/water (10/1). Yield: 95.9%. ^{1}H NMR (400 MHz, CD_3CN, room temperature) δ 8.51 (d, J = 7.7 Hz, 2H), 7.40 (t, J = 7.5 Hz, 2H), 7.34 (t, J = 7.3 Hz, 2H), 7.25 (d, J = 7.4 Hz, 2H), 7.04 (d, J = 8.1 Hz, 1H), 6.81 (s, 1H), 6.72 (d, J = 8.2 Hz, 1H), 4.20 - 4.13 (m, 2H), 4.06 (p, J = 6.9 Hz, 2H), 3.85 -3.76 (m, 2H), 3.71 – 3.63 (m, 2H), 3.59 - 3.49 (m, 2H), 3.34 (s, 3H), 2.83 (t, J = 7.2 Hz, 4H), 2.73 - 2.59 (m, 4H), 1.42 - 1.31 (m, 3H). ^{13}C NMR (100 MHz, CD_3CN, room temperature) δ 149.3, 148.3, 147.4, 137.8, 134.8, 130.0, 129.0, 128.4, 127.3, 126.4, 124.5, 120.6, 113.2, 110.7, 71.3, 69.9, 68.9, 68.1, 63.9, 57.6, 27.2, 25.1, 13.8. ESI-MS m/z: calcd for 521.6460, found 522.2640 ($[M+H]^+$).

Synthesis of tpy-$IrCl_3$

Ssynthesis route was based on literature. [7]

Synthesis of 8C-tpy-$IrCl_3$

Synthesis route of **8C-tpy** was based on literature. [8] Synthesis route of **8C-tpy-**

$IrCl_3$ was similar to **tpy-$IrCl_3$**.

Synthesis of Ir-H

A mixture of the iridium intermediate Ir(tpy)Cl_3 (0.25 g, 0.38 mmol), L (0.20 g, 0.40 mmol) and $AgBF_4$ (0.40 g, 2.00 mmol) was dissolved in 12 mL glycol at a 150 ml shrek bottle. The mixture was heated to 220 ℃ and react overnight under nitrogen atmosphere. After cooling to room temperature, excessive $AgBF_4$ was filtered out and rinse with excessive methanol until no color, collect orange-red solution, spin out methanol solution coarse products was got through pouring into water. The orange solid was purified through column chromatography (CH_2Cl_2/methanol: (100:1, v/v). Yield: 58%. ^{1}H NMR (400 MHz, *d_6*-DMSO, room temperature) δ 8.67 (d, J = 3.2 Hz, 2H), 8.56 (d, J = 7.3 Hz, 2H), 8.39 (s, 2H), 8.09 - 7.99 (m, 1H), 7.94 (q, J = 7.9 Hz, 2H), 7.42 (q, J = 7.2, 5.3 Hz, 2H), 7.33 (t, J = 7.0 Hz, 2H), 7.26 (t, J = 7.4 Hz, 2H), 7.22 - 7.14 (m, 2H), 6.90 (dd, J = 8.1, 3.1 Hz, 1H), 6.82 - 6.68 (m, 1H), 6.65 - 6.56 (m, 1H), 3.97 (p, J = 6.5 Hz, 2H), 2.74 (q, J = 7.4 Hz, 4H), 2.67 - 2.51 (m, 4H), 1.27 (q, J = 6.8, 6.0 Hz, 3H). ^{13}C NMR (100 MHz, *d_6*-DMSO, room temperature) δ 155.6, 155.3, 149.8, 149.7, 148.3, 147.2, 146.9, 138.9, 138.2, 137.9, 135.3, 129.7, 129.2, 128.1, 127.3, 125.2, 124.9, 121.6, 121.2, 116.2, 114.6, 64.4, 27.8, 25.8, 15.2. ESI-MS: calcd for 974.30 g/mol, found 843.25 g/mol ($[M\text{-}BF_4^-]^+$). Elemental analysis: Anal. calcd for $C_{44}H_{34}N_4O_2Ir$, C: 62.69, H: 4.07, N: 6.65. Found C: 62.85 (Laboratory error: 0.26%), H: 4.058 (Laboratory error: 0.29%), N: 6.671 (Laboratory error: 0.32%).

Synthesis of Ir-8C

Complex **Ir-8C** was synthesized with a similar route of **Ir-H** with using iridium intermediate 8C-Ir(tpy)Cl_3. Yield: 56%. ^{1}H NMR (400 MHz, *d_6*-DMSO, room temperature) δ 1H NMR (400 MHz, DMSO-d6) δ 8.69 - 8.52 (m, 1H), 8.37 (d, J = 7.7 Hz, 2H), 8.01 - 7.87 (m, 1H), 7.45 (t, J = 7.4 Hz, 1H), 7.35 (d, J = 7.5, 2H), 7.28 (t, J = 7.2 Hz, 2H), 7.22 (d, J = 7.4 Hz, 2H), 6.89 (d, J = 7.9 Hz, 1H), 6.79 - 6.72 (m, 1H), 6.61 (d, J = 8.0 Hz, 1H), 3.98 (q, J = 6.9 Hz, 4H), 2.76 (t, J = 7.2 Hz, 8H), 1.36 - 1.12 (m, 12H), 1.02 (t, J = 7.0 Hz, 3H), 0.91 - 0.73 (m, 3H). ^{13}C NMR (100 MHz, *d_6*-DMSO, room temperature) δ 167.3, 157.2, 155.4, 149.8, 149.7, 148.3, 147.2, 147.1, 138.2, 137.9, 135.3, 129.7, 128.2, 128.0, 127.4, 125.2, 125.0, 121.7, 121.4, 116.2, 114.6,

107.3, 68.5, 64.4, 31.8, 29.1, 28.9, 27.9, 25.9, 22.6, 19.1, 15.2, 14.5. Matrix assisted laser desorption ionization time of flight mass spectrometry (MALDI-TOF-MS): calcd for 1102.42 g/mol, found 971.35 g/mol ([M-BF_4^-]$^+$). Elemental analysis: Anal. calcd for $C_{52}H_{50}N_4O_3Ir$, C: 64.31. H: 5.19, N: 5.77. Found C: 64.16 (Laboratory error: 0.23%), H: 5.203 (Laboratory error: 0.25%), N: 5.787 (Laboratory error: 0.29%).

Synthesis of Ir-O

Complex **Ir-O** was synthesized with a similar route of **Ir-H** with using ligand **L-O**. Yield: 54%. ^{1}H NMR (400 MHz, *d_6*-DMSO, room temperature) δ ^{1}H NMR (400 MHz, *d_6*-DMSO) δ 8.59 (d, J = 7.5 Hz, 2H), 8.21(s, 2H), 8.12 (d, J = 7.2 Hz, 2H), 7.71 (d, J = 7.4 Hz, 2H), 7.83 (t, J = 7.3 Hz, 1H), 7.59 (t, J = 8.3 Hz, 2H), 7.08 (d, J = 6.0 Hz, 2H), 7.02 (d, J = 8.2 Hz, 2H), 6.88 (d, J = 7.3 Hz, 2H), 6.72 (d, J = 5.2 Hz, 1H), 6.67 (t, J = 4.9 Hz, 1H), 6.55 (d, J = 8.1 Hz, 1H), 4.23 - 4.11 (m, 2H), 4.04 (q, J = 6.9 Hz, 2H), 3.68 - 3.60 (m, 2H), 3.61 - 3.51 (m, 4H), 3.45 (td, J = 11.5, 9.6, 5.5 Hz, 3H), 2.81 (t, J = 7.1 Hz, 4H), 2.64 (t, J = 8.4 Hz, 4H), 1.31 (t, J = 6.9 Hz, 3H).^{13}C NMR (100 MHz, *d_6*-DMSO, room temperature) δ 149.2, 148.1, 147.7, 147.4, 137.7, 134.7, 129.5, 129.0, 128.7, 127.6, 126.8, 124.6, 120.9, 114.1, 113.7, 71.3, 68.9, 68.2, 65.5, 63.9, 58.0, 27.3, 25.3, 15.1, 14.6. Matrix assisted laser desorption ionization time of flight mass spectrometry (MALDI-TOF-MS): calcd for 945.30 g/mol, found 945.64 g/mol ([M-BF_4^-]$^+$). Elemental analysis: Anal. calcd for $C_{49}H_{44}N_4O_4Ir$, C: 62.27. H: 4.69, N: 5.93. Found C: 62.40 (Laboratory error: 0.21%), H: 4.677 (Laboratory error: 0.28%), N: 5.913 (Laboratory error: 0.29%).

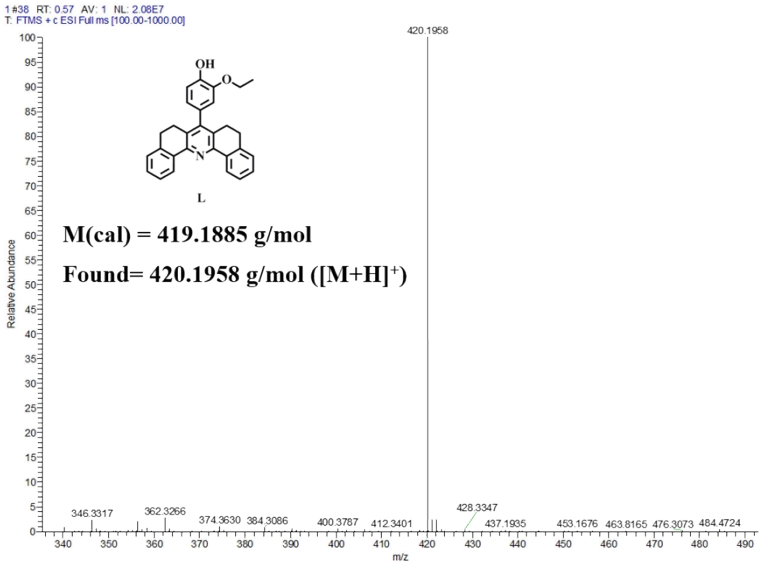

Figure S1 ESI-Mass spectrum of **L**.

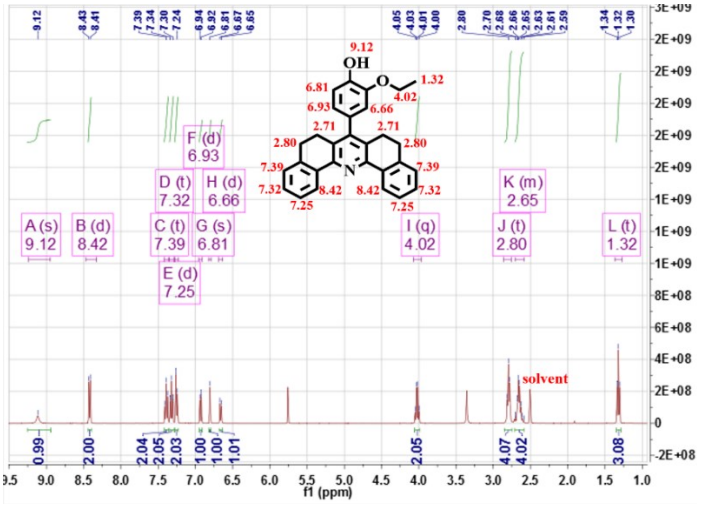

Figure S2 ^{1}H NMR spectrum (400 MHz, d_6-DMSO, room temperature) of **L**.

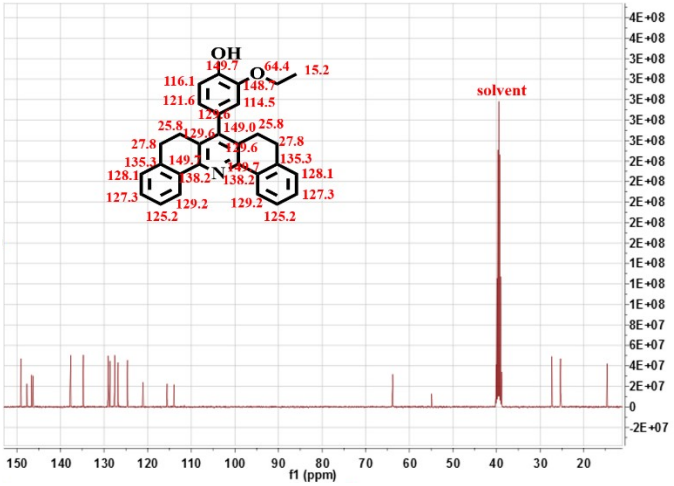

Figure S3 ^{13}C NMR spectrum (100 MHz, d_6-DMSO, room temperature) of **L**.

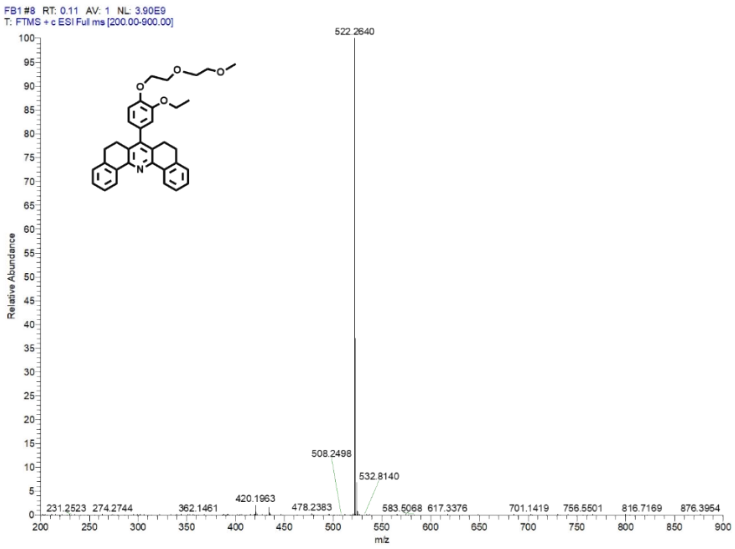

Figure S4 ESI-Mass spectrum of **L-O**.

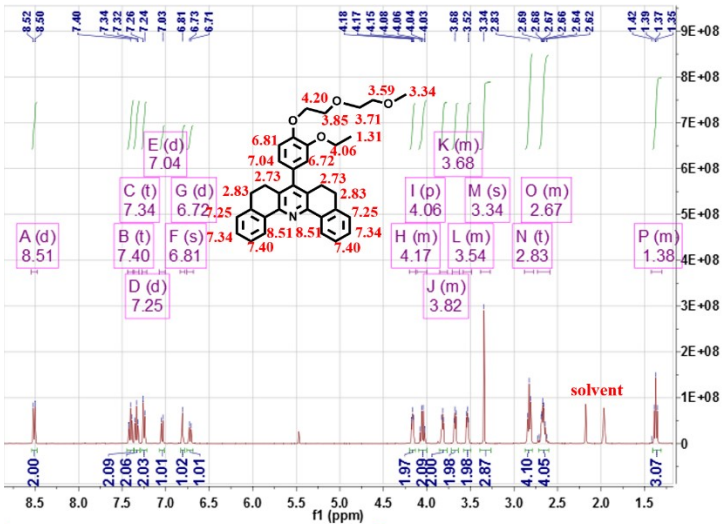

Figure S5 ^{1}H NMR spectrum (400 MHz, CD_3CN, room temperature) of **L-O**.

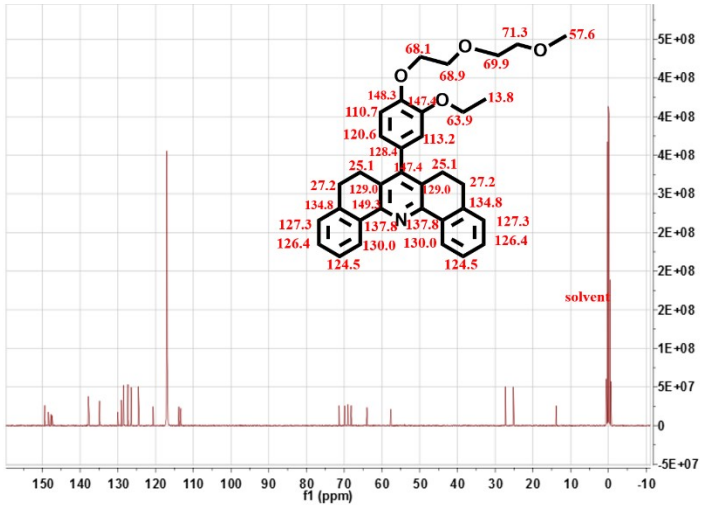

Figure S6 ^{13}C NMR spectrum (100 MHz, CD_3CN, room temperature) of **L-O**.

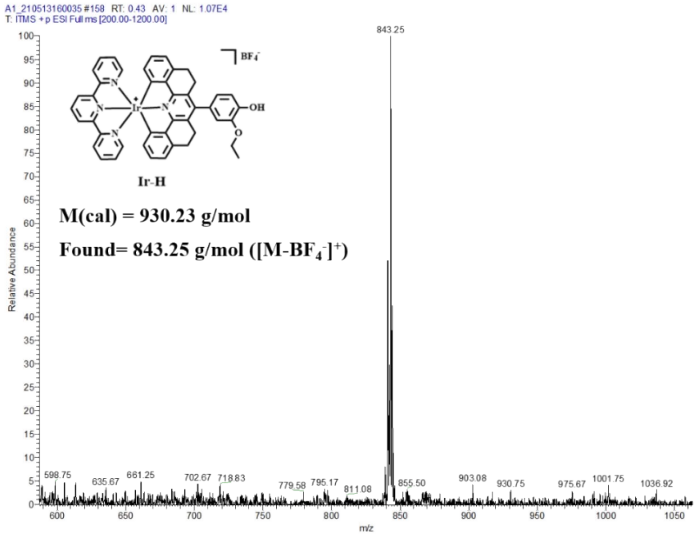

Figure S7 ESI-Mass spectrum of **Ir-H**.

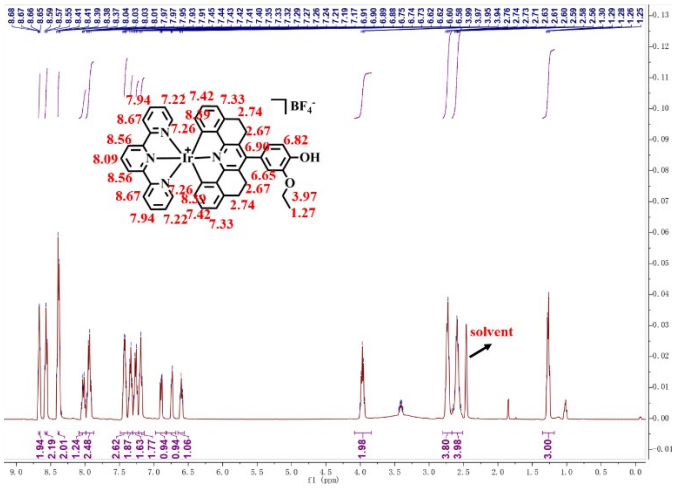

Figure S8 ^{1}H NMR spectrum (400 MHz, d_6-DMSO, room temperature) of **Ir-H**.

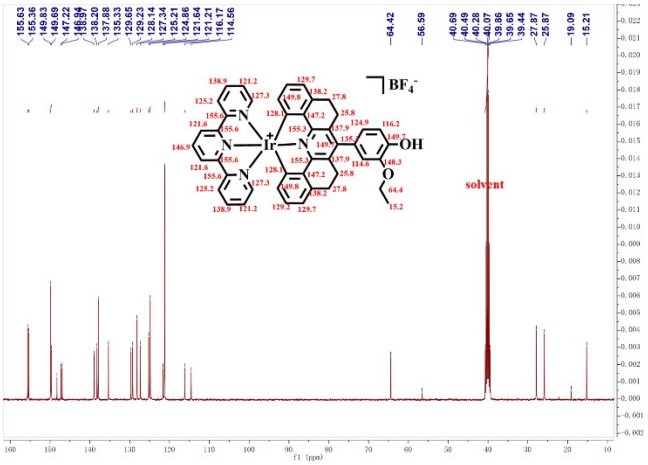

Figure S9 ^{13}C NMR spectrum (100 MHz, d_6-DMSO, room temperature) of **Ir-H**.

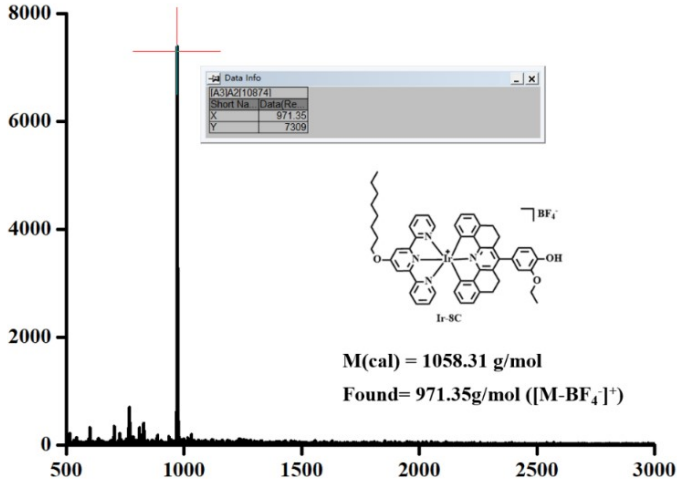

Figure S10 MALDI-TOF-MS spectrum of **Ir-8C**.

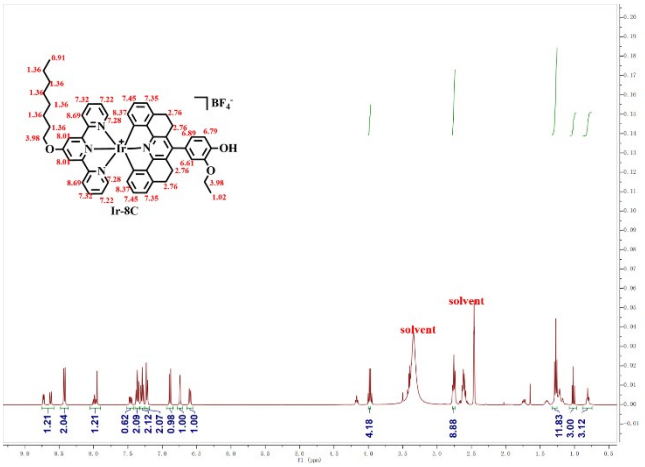

Figure S11 ^{1}H NMR spectrum (400 MHz, d_6-DMSO, room temperature) of **Ir-8C**.

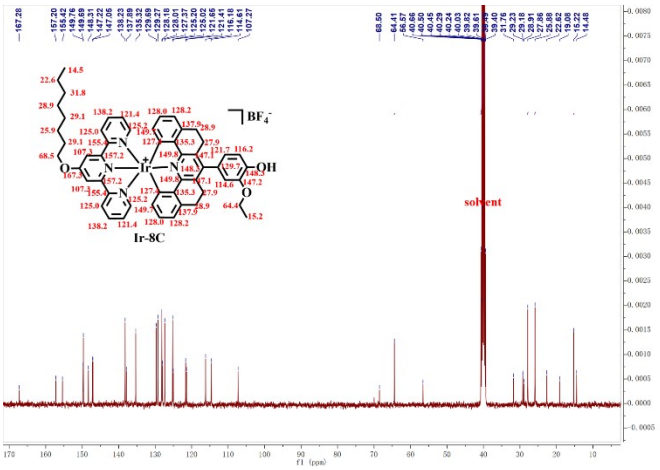

Figure S12 ^{13}C NMR spectrum (100 MHz, d_6-DMSO, room temperature) of **Ir-8C**.

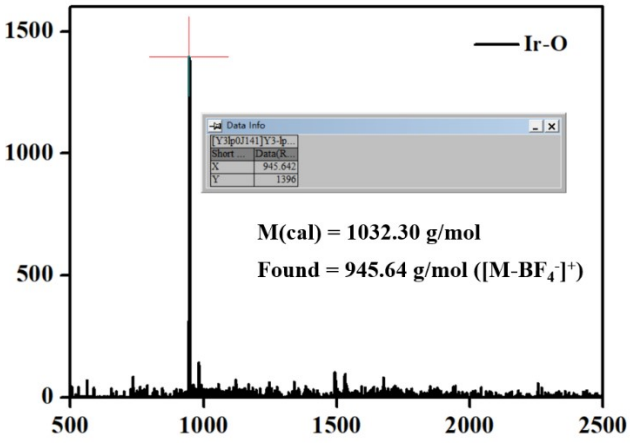

Figure S13 MALDI-TOF-MS spectrum of **Ir-O**.

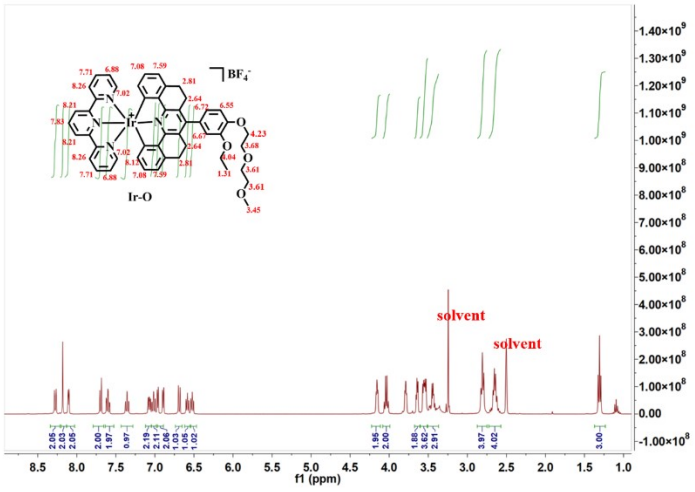

Figure S14 ^{1}H NMR (400 MHz, d_6-DMSO, room temperature) spectrum of **Ir-O**.

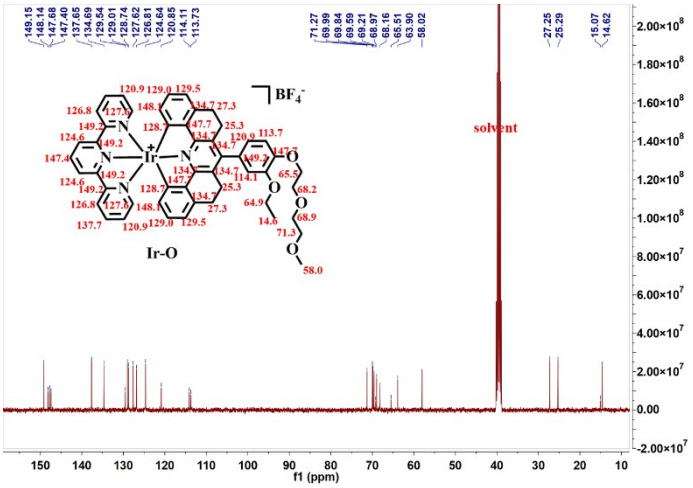

Figure S15 ^{13}C NMR spectrum (100 MHz, d_6-DMSO, room temperature) of **Ir-O**.

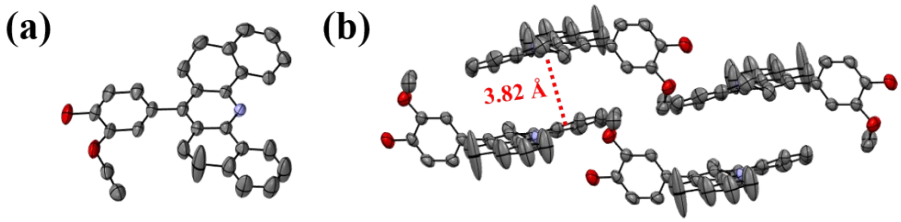

Figure S16 (a) Single crystal of **L**. (b) Packing mode of **L** (H atoms are omitted for clarity).

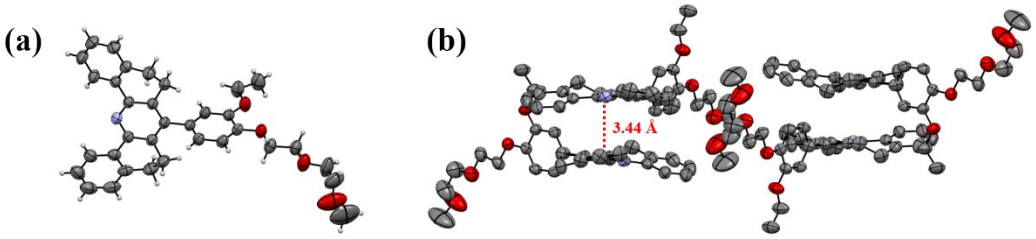

Figure S17 (a) Single crystal of **L-O**. (b) Packing mode of **L-O** (H atoms are omitted for clarity).

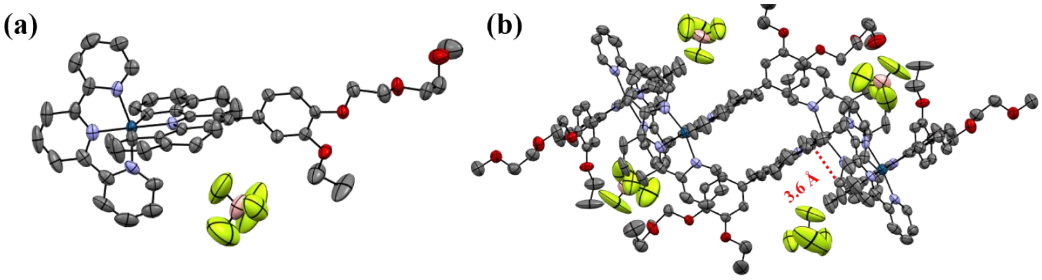

Figure S18 (a) Single crystal of **Ir-O**. (b) Packing mode of **Ir-O** (H atoms are omitted for clarity).

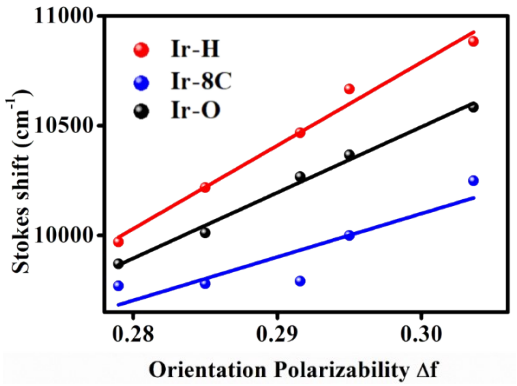

Figure S19 Lippert-Mataga plots for **Ir-H**, **Ir-8C** and **Ir-O**.

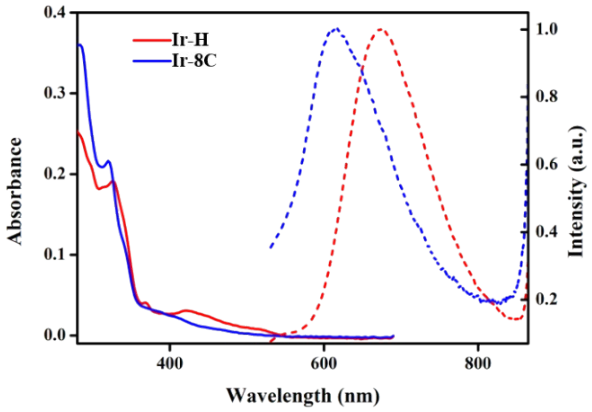

Figure S20 UV-*vis* and fluorescence spectra of **Ir-H** and **Ir-8C** (Red: **Ir-H**, Blue: **Ir-8C**. Concentration: 1 × 10^{-5} mol/L. Solvent: DMSO.).

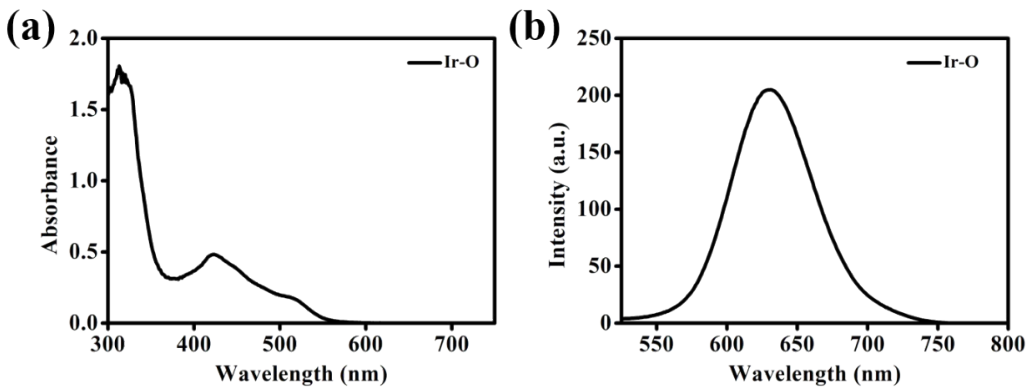

Figure S21 (a) UV-*vis* and (b) fluorescence spectra of **Ir-O** (Concentration: 1 × 10^{-5} mol/L. Solvent: DMSO.).

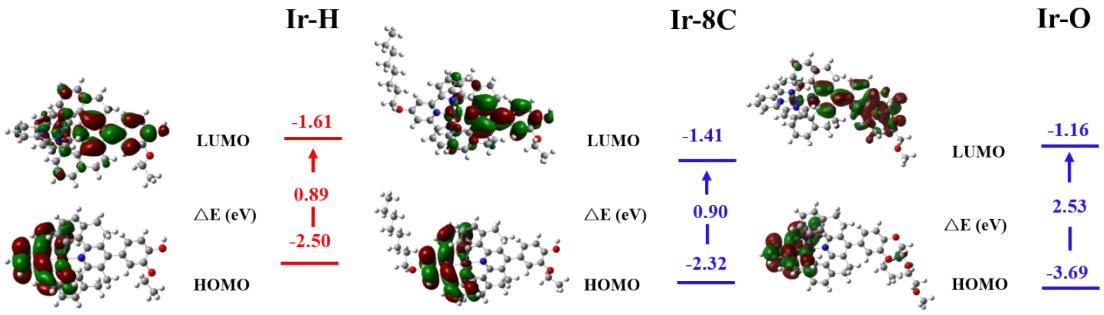

Figure S22 Highest occupied molecular orbital (HOMO) and lowest unoccupied molecular orbital (LUMO) energy levels of **Ir-H**, **Ir-8C** and **Ir-O**.

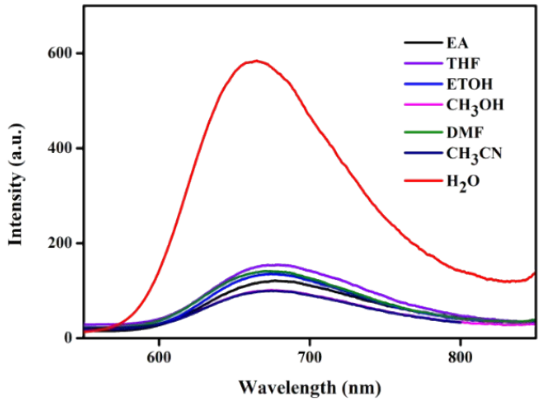

Figure S23 Fluorescence spectra of **Ir-H** in different polarity of solvents. (Concentration: 1 ✍ 10^{-4} mol/L. Solvents including: ethyl acetate, tetrahydrofuran, ethanol, methanol, N, N-dimethylformamide, acetonitrile and water.)

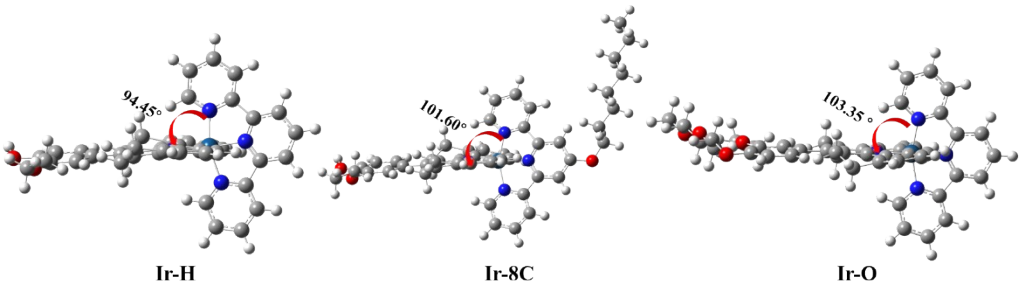

Figure S24 Distorted structure of **Ir-H**, **Ir-8C**, and **Ir-O**.

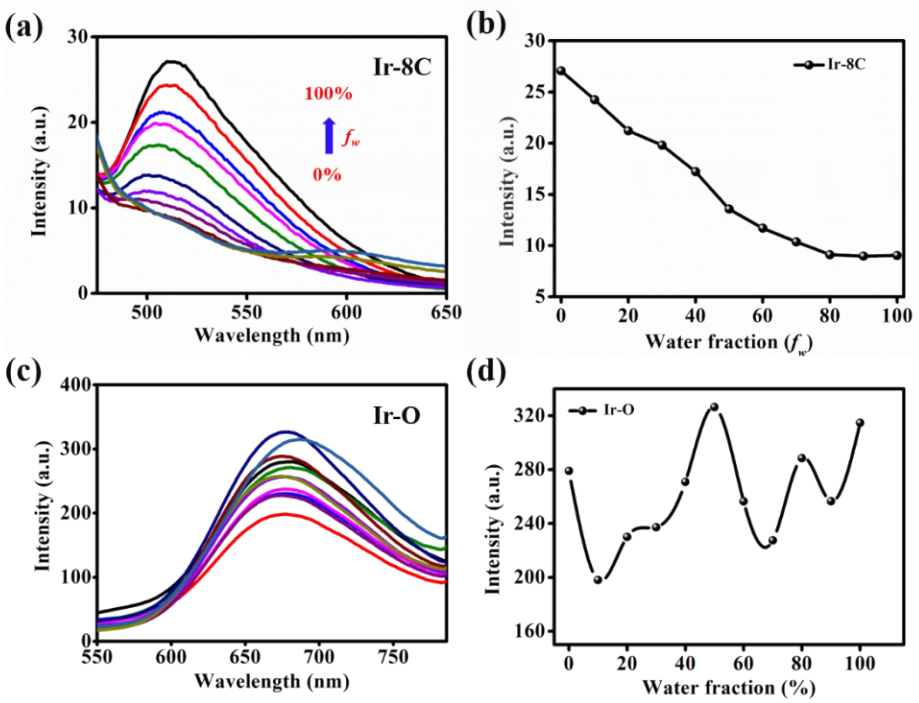

Figure S25 Fluorescence spectra of (a) **Ir-8C** and (b) **Ir-O** with water fraction increased (Concentration: 1 ∽ 10^{-5} mol/L. Solvent: f_w = 0%, 10%, 20%, 30%, 40%, 50%, 60%, 70%, 80%, 90% and 100%).

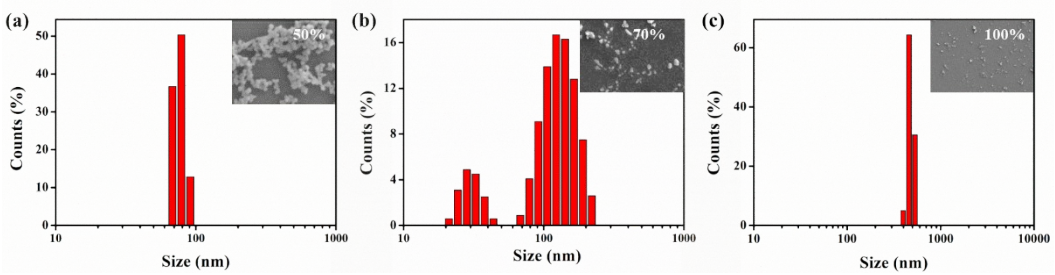

Figure S26 Dynamic light scattering (DLS) and scanning electron microscope (SEM) results of **Ir-H** in different water fraction. (a) f_w = 50%. (b) f_w = 70%. (c) f_w = 100%.

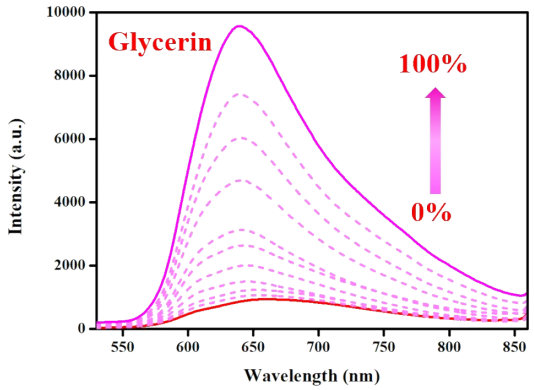

Figure S27 Fluorescence spectra of **Ir-H** with different fraction of glycerin (Concentration: 1 ≀ 10^{-5} mol/L. Solvent: $f_{glycerin}$ = 0%, 10%, 20%, 30%, 40%, 50%, 60%, 70%, 80%, 90% and 100%).

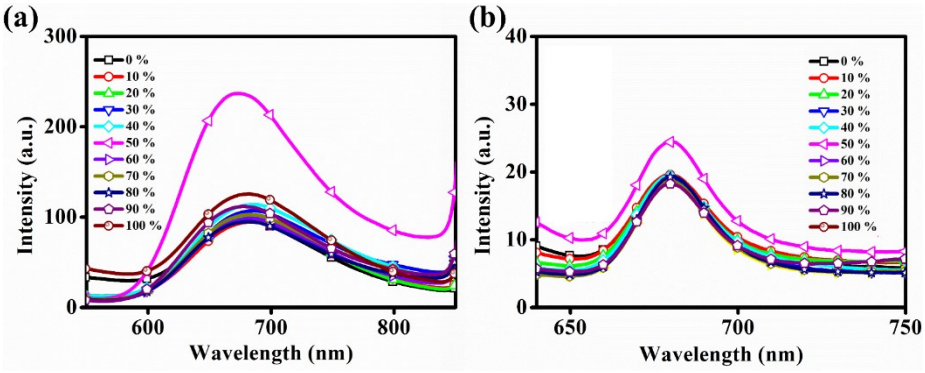

Figure S28 Fluorescence spectra of **Ir-H** with different phosphate buffer saline fraction (0%, 10%, 20%, 30%, 40%, 50%, 60%, 70%, 80%, 90% and 100%) in concentration of (a) 2 ≀ 10^{-6} mol/L and (b) 2 ≀ 10^{-7} mol/L. The inserted figures: linear graphs for fluorescence intensity.

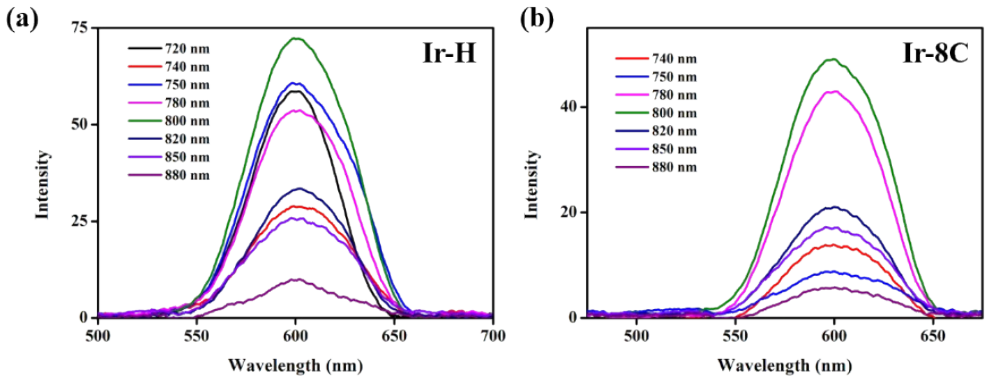

Figure S29 Two-photon fluorescence spectra of (a) **Ir-H** and (b) **Ir-8C** in wavelength range 720-880 nm (Concentration: 1 mM. Solvent: DMSO.).

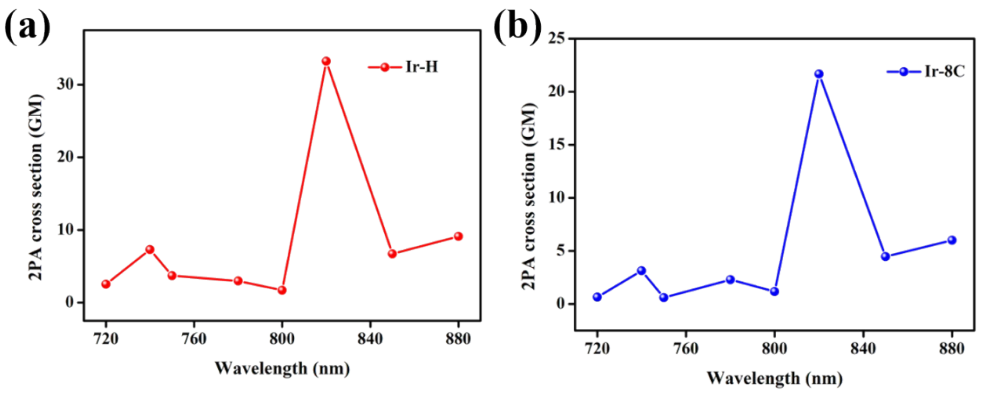

Figure S30 Two-photon absorption cross section of (a) **Ir-H** and (b) **Ir-8C** in wavelength range 720-880 nm (Concentration: 1 mM. Solvent: DMSO.).

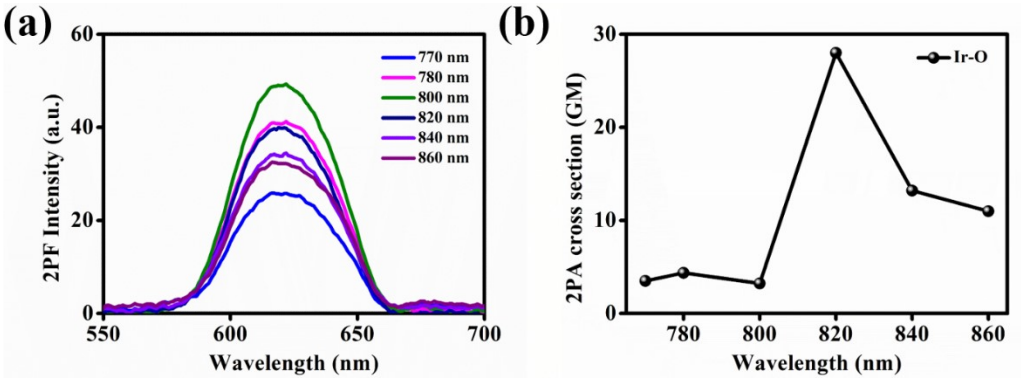

Figure S31 (a) Two-photon excited fluorescence spectra and (b) Two-photon absorption cross section of **Ir-O** in wavelength range 770-880 nm (Concentration: 1 mM. Solvent: d DMSO.).

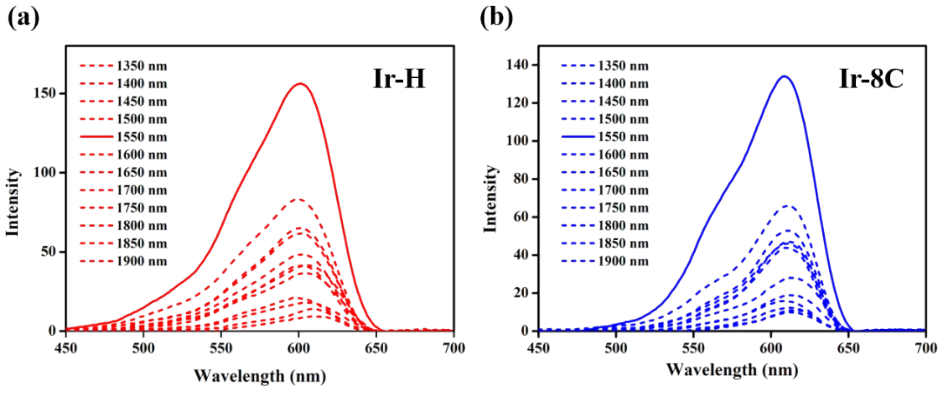

Figure S32 Three-photon fluorescence spectra of (a) **Ir-H** and (b) **Ir-8C** in wavelength range 1350-1900 nm (Concentration: 1 mM. Solvent: DMSO.).

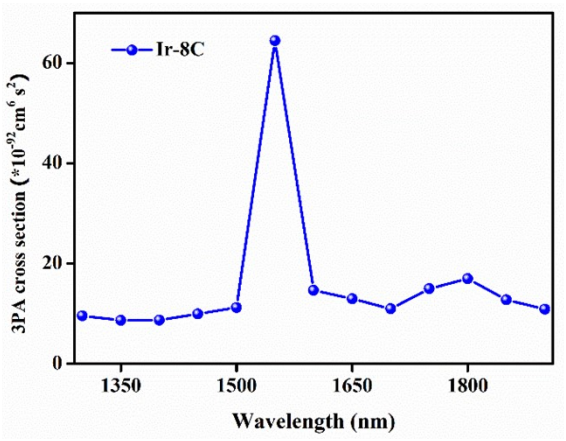

Figure S33 Three-photon absorption cross section of **Ir-8C** in wavelength range 1350-190 nm (Concentration: 1 mM. Solvent: DMSO.).

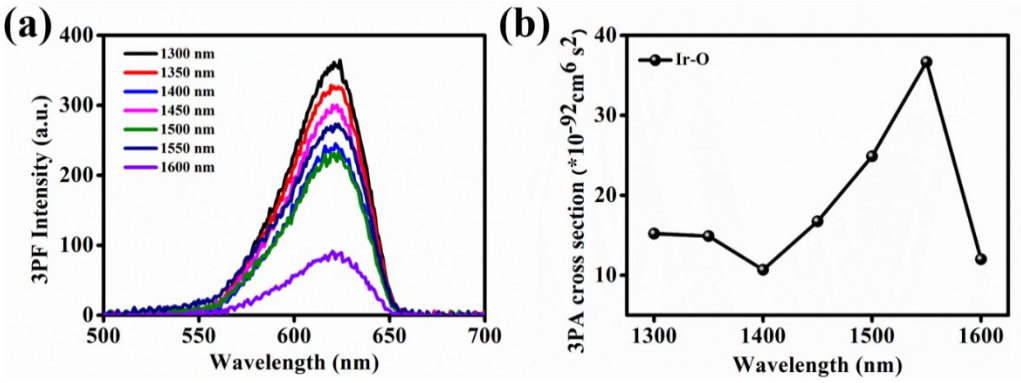

Figure S34 (a) Three-photon excited fluorescence spectra and (b) Three-photon absorption cross section of **Ir-O** in wavelength range 1300 - 1600 nm (Concentration: 1 mM. Solvent: DMSO.).

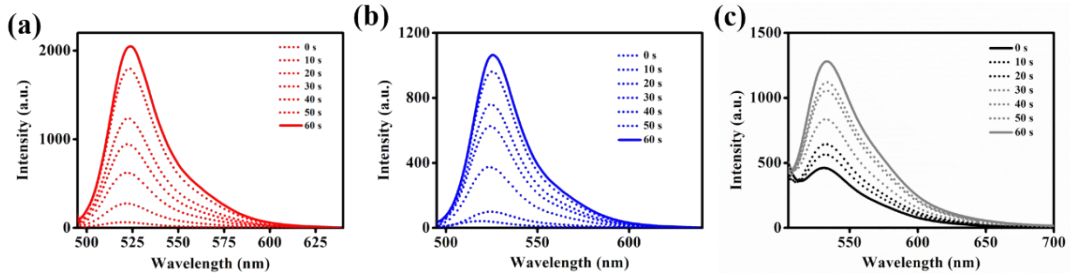

Figure S35 Fluorescence of DCFH-DA with prolonged laser irradiation time. (Solvent: phosphate buffer saline. With adding (a) **Ir-H**, (b) **Ir-8C** and (c) **Ir-O**. Concentration: 1 mM.).

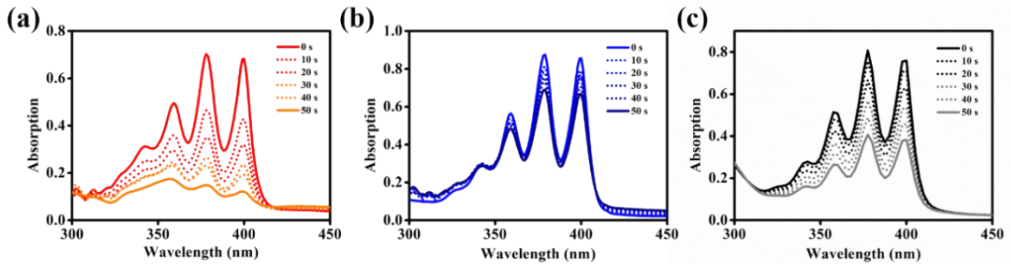

Figure S36 Absorption spectra of ABDA with prolonged laser irradiation time. (Solvent: phosphate buffer saline. With adding (a) **Ir-H** (b) **Ir-8C** and (c) **Ir-O**. Concentration: 1 mM.).

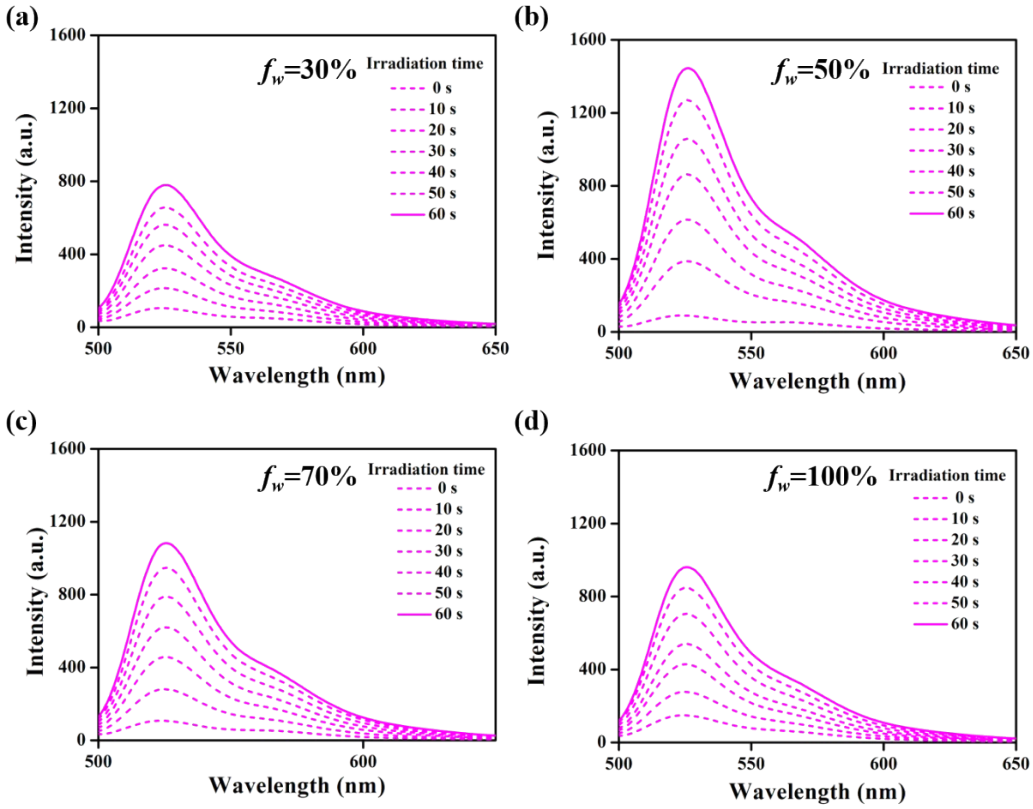

Figure S37 Fluorescence of DCFH in the presence of **Ir-H** with prolonged laser irradiation time in DMSO/H_2O mixtures with different water fractions (Solvent: a: f_w = 30%; b: f_w = 50%; c: f_w = 70%; d: f_w = 100%. Concentration: 1 mM.).

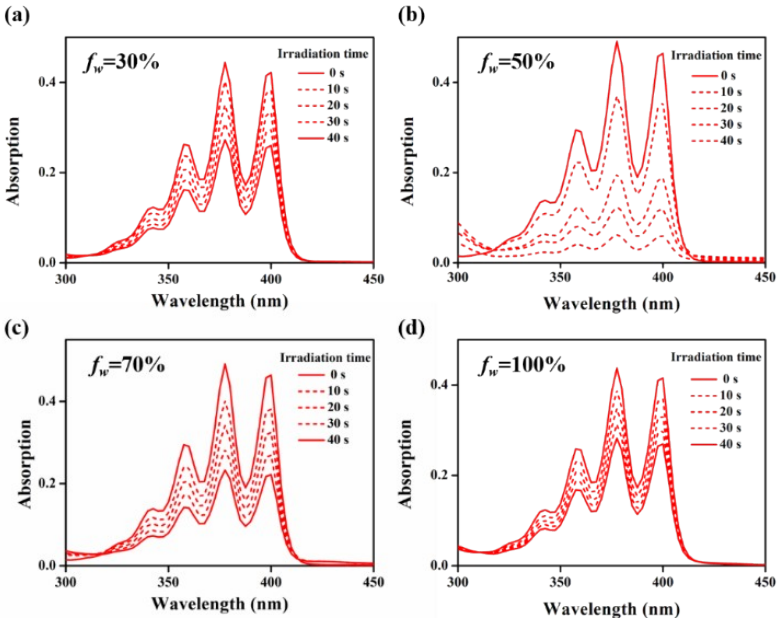

Figure S38 Absorption spectra of ABDA in the presence of **Ir-H** with prolonged laser irradiation time in DMSO/H_2O mixtures with different water fractions (Solvent: a: f_w = 30%, b: f_w = 50%, c: f_w = 70%, d: f_w = 100%. Concentration: 1 mM.).

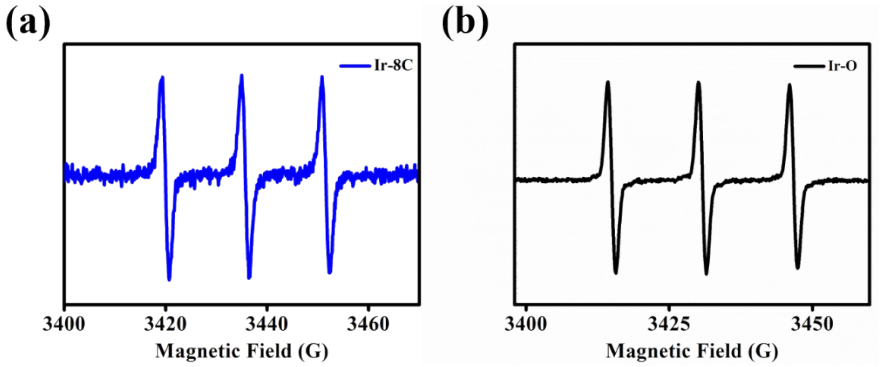

Figure S39 Electron paramagnetic resonance spectra of (a) **Ir-8C** and(a) **Ir-O** under light irradiation.

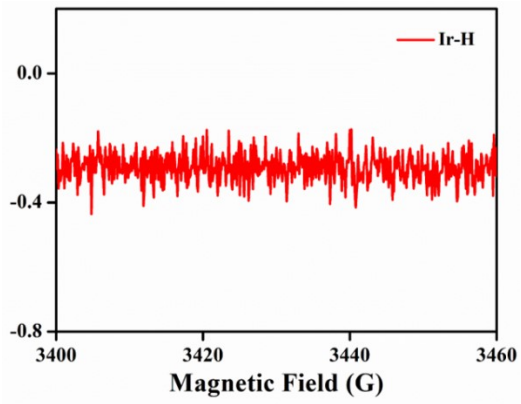

Figure S40 Electron paramagnetic resonance spectra of **Ir-H** under light irradiation.

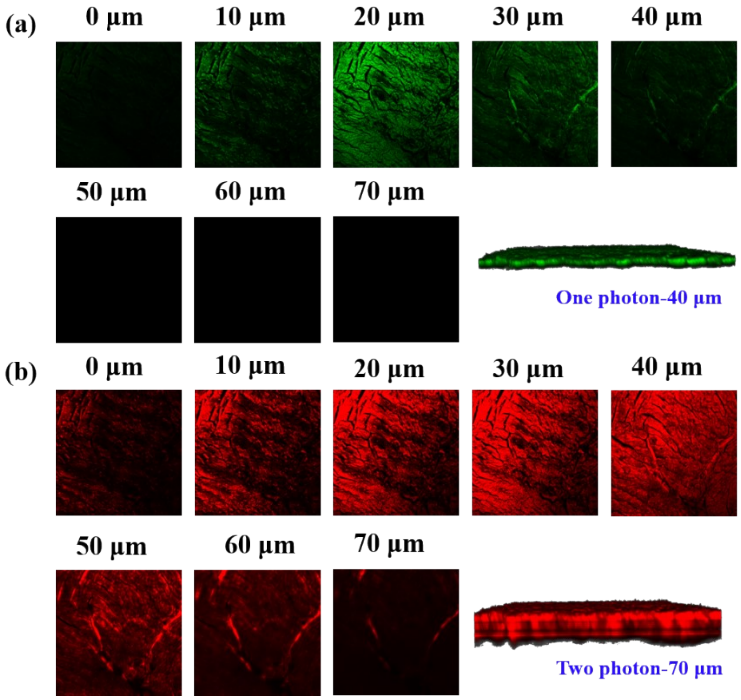

Figure S41 (a) One-photon (405 nm) and (b) two-photon (820 nm) fluorescence images of tissue section incubated with **Ir-H** (1 M, 15 min) with different penetration depth along the z axis.

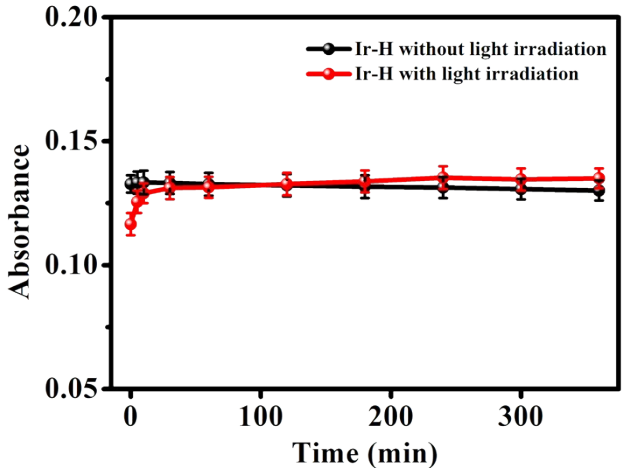

Figure S42 Stability of **Ir-H** in phosphate buffer saline with and without light irradiation (Concentration: 2 μ 10^{-6} mol/L).

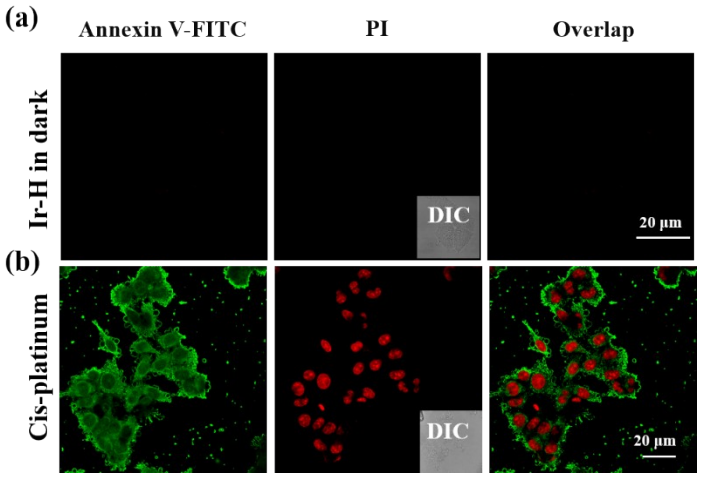

Figure S43 Photodynamic therapy efficacy of **Ir-H** incubated (2 μM) Hep G2 cells treated with Annexin V-FITC/PI (5 μM) without laser irradiation. (FITC: λ_{ex} = 488 nm, λ_{em} = 525 nm. PI: λ_{ex} = 514 nm, λ_{em} = 615 nm). (b) Cis-platinum can induce apoptosis through chemotherapy approach which was used as a positive control (10 μg/mL).

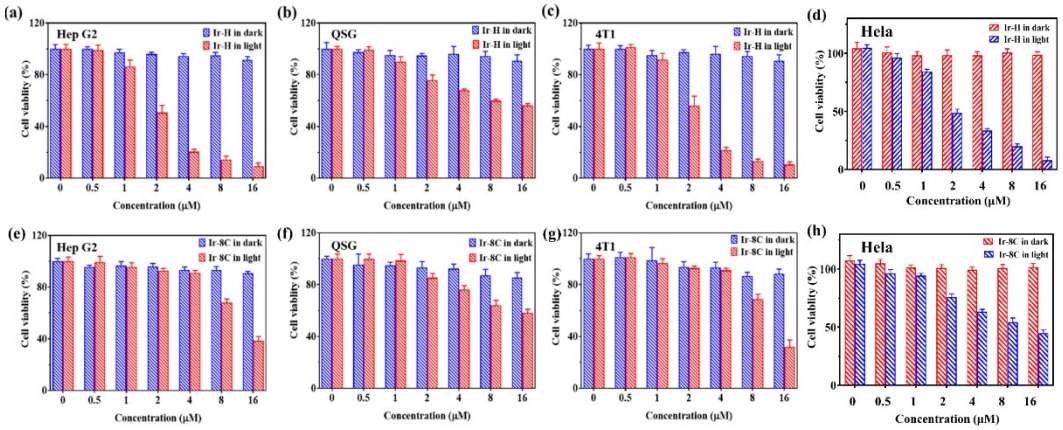

Figure S44 Cell toxicity results under dark and light conditions incubated with different concentration of **Ir-H** and **Ir-8C** (0.5 μM, 1 μM, 2 μM, 4 μM, 8 μM, 16 μM) in dark and in laser condition using different cell lines. (a) **Ir-H** incubated with Hep G2 cell. (b) **Ir-H** incubated with QSG cell. (c) **Ir-H** incubated with 4T1 cell. (d) **Ir-H** incubated with Hela cell. (e) **Ir-8C** incubated with Hep G2 cell. (f) **Ir-8C** incubated with QSG cell. (g) **Ir-8C** incubated with 4T1 cell. (h) **Ir-8C** incubated with Hela cell.

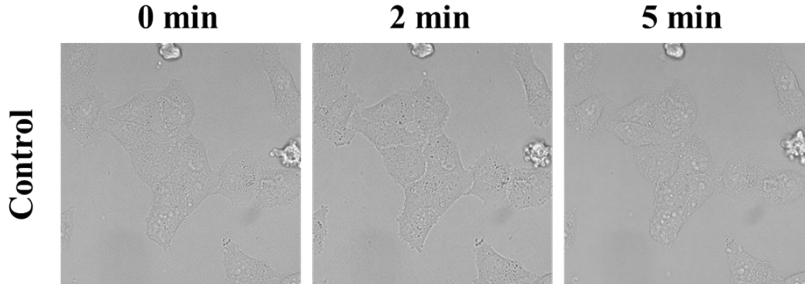

Figure S45 Bright field of Hep G2 cells under laser irradiation for different time (Laser: 820 nm. Irradiation time: 0 min, 2 min and 5 min) without adding probe.

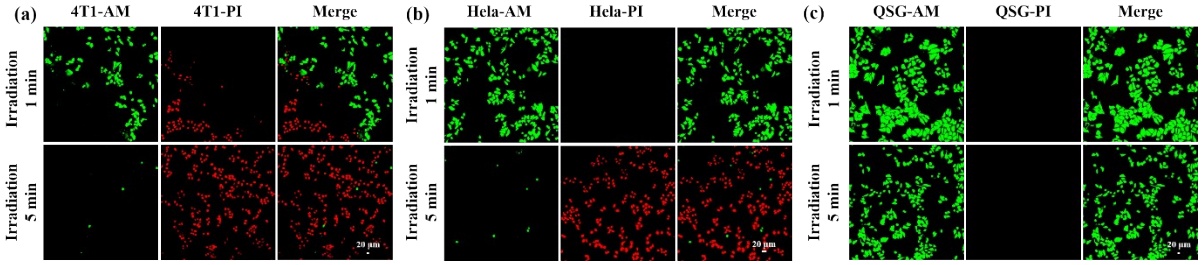

Figure S46 (a) 4T1, (b)Hela and (c) QSG cells toxicity using Calcein-AM/PI as apoptosis indicator of **Ir-H** (Concentration: 2 μM. Light: 820 nm laser. AM: λ_{ex} = 488 nm, λ_{em} = 525 nm. PI: λ_{ex} = 514 nm, λ_{em} = 615 nm. Scale bar:20 μm).

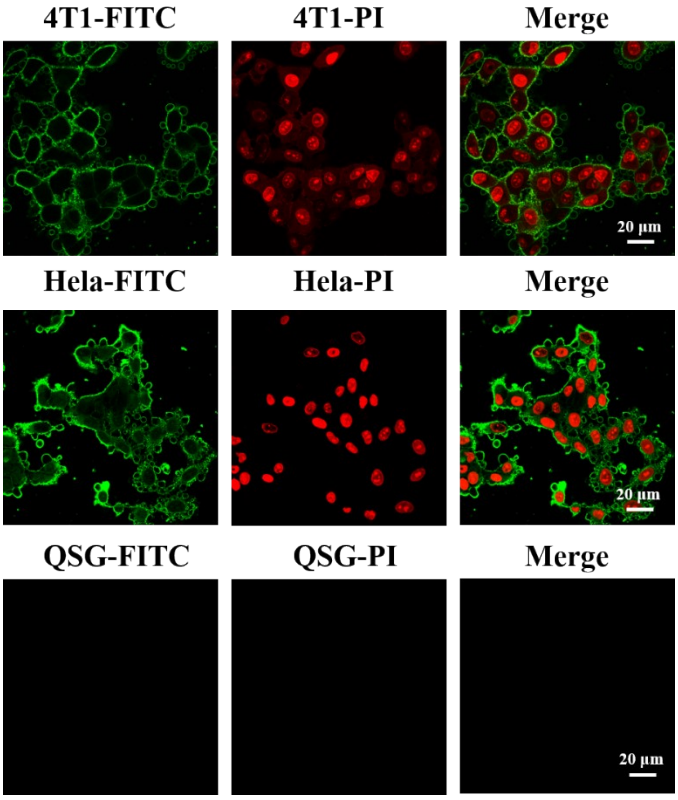

Figure S47 4T1, Hela and QSG cell lines incubated with **Ir-H** using Annexin V-FITV/PI as cell apoptosis indicator (Concentration: 2 μM. Light: 820 nm laser. FITC: λ_{ex} = 488 nm, λ_{em} = 525 nm. PI: λ_{ex} = 514 nm, λ_{em} = 615 nm. Scale bar:20 μm).

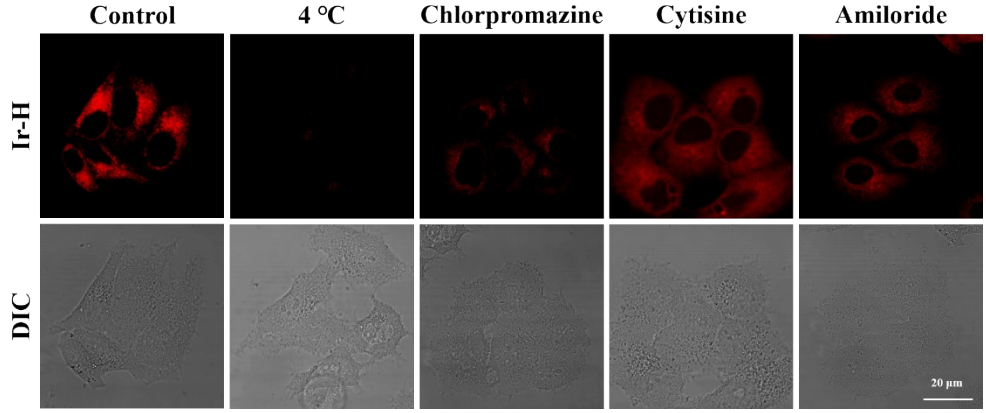

Figure S48 Confocal images of Hep G2 cells incubated with different endocytic inhibitors: low temperature (4 °C), chlorpromazine (100 μg/mL), cytisine (200 μg/mL) and amiloride (200 μg/mL). The cells were pretreated with 2 μM of **Ir-H** for 30 min.

Table S1 Crystal data and structure refinement for L.

Identification code	**L**
Empirical formula	$C_{29}H_{25}NO_2$
Formula weight	419.05
CCDC number	2106416
Temperature/K	296.15
Crystal system	monoclinic
Space group	$P2_1/c$
a/Å	7.124(2)
b/Å	33.014(11)
c/Å	9.273(3)
α/°	90
β/°	93.355(4)
γ/°	90
Volume/Å^3	2177.3(12)
Z	4
ρ_{calc}g/cm^3	1.280
μ/mm^{-1}	0.080
F(000)	888.0
Crystal size/mm^3	0.29 × 0.26 × 0.2
Radiation	MoKα (λ = 0.71073)
2Θ range for data collection/°	4.57 to 54.778
Index ranges	$-9 \le h \le 9$, $-42 \le k \le 33$, $-11 \le l \le 11$
Reflections collected	16716
Independent reflections	4514 [R_{int} = 0.0511, R_{sigma} = 0.0506]
Data/restraints/parameters	4514/221/364
Goodness-of-fit on F^2	1.022
Final R indexes [I>=2σ (I)]	R_1 = 0.0602, wR_2 = 0.1392
Final R indexes [all data]	R_1 = 0.1137, wR_2 = 0.1634
Largest diff. peak/hole / e Å^{-3}	0.14/-0.16

Table S2 Crystal data and structure refinement for L-O.

Identification code	**L-O**
Empirical formula	$C_{34}H_{35}NO_4$
Formula weight	521.26
CCDC number	2132903
Temperature/K	296.15
Crystal system	monoclinic
Space group	$P2_1/c$

a/Å	9.1797(13)
b/Å	30.203(4)
c/Å	11.0131(16)
α/°	90.00
β/°	111.056(2)
γ/°	90.00
Volume/Å^3	2849.6(7)
Z	57
ρ_{calc}g/cm^3	1.429
μ/mm^{-1}	0.128
F(000)	1254.0
Crystal size/mm^3	0.02 × 0.03 × 0.02
Radiation	MoKα (λ = 0.71073)
2Θ range for data collection/°	2.7 to 54.7
Index ranges	-11 ≤ h ≤ 11, -38 ≤ k ≤ 38, -14 ≤ l ≤ 13
Reflections collected	22024
Independent reflections	5934 [R_{int} = 0.0437, R_{sigma} = 0.0348]
Data/restraints/parameters	5934/0/354
Goodness-of-fit on F^2	1.051
Final R indexes [I>=2σ (I)]	R_1 = 0.0729, wR_2 = 0.2099
Final R indexes [all data]	R_1 = 0.0959, wR_2 = 0.2327
Largest diff. peak/hole / e Å^{-3}	0.94/-0.45

Table S3 Crystal data and structure refinement for Ir-O.

Identification code	**Ir-O**
Empirical formula	$C_{49}H_{44}BF_4IrN_4O_4$
Formula weight	1031.91
CCDC number	2132913
Temperature/K	296.15
Crystal system	monoclinic
Space group	$P2_1/c$
a/Å	14.904(2)
b/Å	16.186(3)
c/Å	19.171(4)
α/°	90
β/°	112.561(2)
γ/°	90
Volume/Å^3	4270.8(13)
Z	4

ρ_{calc}g/cm^3	1.605
μ/mm^{-1}	3.195
F(000)	2064.0
Crystal size/mm^3	0.01 × 0.01 × 0.02
Radiation	MoKα (λ = 0.71073)
2Θ range for data collection/°	2.96 to 54.798
Index ranges	-18 ≤ h ≤ 19, -15 ≤ k ≤ 20, -23 ≤ l ≤ 15
Reflections collected	32678
Independent reflections	8783 [R_{int} = 0.0695, R_{sigma} = 0.0728]
Data/restraints/parameters	8783/0/570
Goodness-of-fit on F^2	1.015
Final R indexes [I>=2σ (I)]	R_1 = 0.0439, wR_2 = 0.0900
Final R indexes [all data]	R_1 = 0.0864, wR_2 = 0.1042
Largest diff. peak/hole / e Å^{-3}	1.09/-0.73

Table S4 Photophysical data of the **Ir-H**, **Ir-8C** and **Ir-O**.

	Solvents	λ_{abs} (nm)[a]	λ_{em} (nm)[b]	❒v(nm)[c]	Φ[d]
Ir-H	DMSO	382	672	290	1.4
Ir-8C	DMSO	422	616	194	0.98
Ir-O	DMSO	420	620	200	1.2

[a] Absorption peak position in DMSO (1×10^{-5} mol L^{-1}). [b] Emission band in DMSO (1.0×10^{-5} mol L^{-1}), excited at the absorption maximum. [c] Stokes shift [d] Quantum yields.

Table S5 Singlet oxygen generation quantum yield comparison between **Ir-H** and other reported probes.

Probes	Singlet oxygen generation quantum yield (%)	Ref.
IrDAD	14.6	[9]
L2b NPs and **L2c NPs**	0.401 and 0.355	[10]
ZnL1	72	[11]
Ir-H in f_w = 50% solution	87	This work

Table S6 Energy gap between S1 state and T1 state (ΔE_{ST}) of Ir-H in soluble and aggregate state using time-dependent density functional theory.

	❒E_{ST} in soluble (eV)	❒E_{ST} in aggregate (eV)
Ir-H	2.32	0.45

Table S7 IC_{50} values and photocytotoxicity indices (PI) of **Ir-H** and **Ir-8C** from MTT assay.

IC_{50}	Hep G2		
	light	dark	PI
Ir-H	2.532	130	51.343
Ir-8C	13.419	46.722	3.482

Reference

[1] Zhang, Q.; Lu, X.; Wang, H.; T, X.; Wang, A.; Zhou, H.; Wu, J.; Tian, Y. A benzoic acid terpyridine-based cyclometalated iridium(iii) complex as a two-photon fluorescence probe for imaging nuclear histidine. *Chem. Commun.*, **2018**, 54, 3771-3774.

[2] Zheng, Z.; Zhang, T.; Liu, H.; Chen, Y.; Kwok, R. T. K.; Ma, C.; Zhang, P.; Sung, H. H. Y.; Williams, I. D.; Lam, J. W. Y.; Wong, K. S.; Tang, B. Z. Bright Near-Infrared Aggregation-Induced Emission Luminogens with Strong Two-Photon Absorption, Excellent Organelle Specificity, and Efficient Photodynamic Therapy Potential. *ACS Nano*, **2018**, 12, 8145-8159.

[3] Li, M.; Xia, J.; Tian, R.; Wang, J.; Fan, J.; Du, J.; Long, S.; Song, X.; Foley, J. W.; Peng, X. Near-Infrared Light-Initiated Molecular Superoxide Radical Generator: Rejuvenating Photodynamic Therapy against Hypoxic Tumors. *J. Am. Chem. Soc.*, **2018**, 140, 14851-14859.

[4] Ni B., Cao H. Z., Zhang C. K., Li S. L., Zhang Q., Tian X. H., Li D. D., Wu J. Y., and Tian Y. P. Activated Type I and Type II Process for Two-Photon Promoted ROS Generation: The Coordinated Zn Matters. *Inorg. Chem.*, **2020**, 59, 13671-13678.

[5] Dong, Y.; Dong, S.; Wang, Z.; Feng, L.; Sun, Q.; Chen, G.; He, F.; Liu, S.; Li, W.; Yang, P. Multimode Imaging-Guided Photothermal/Chemodynamic Synergistic Therapy Nanoagent with a Tumor Microenvironment Responded Effect. *ACS Appl. Mater. Interfaces*, **2020**, 12, 52479-52491.

[6] Li B., Cao H. Z. Zheng J., Ni B., Lu X., Tian X. H., Tian Y. P. and Li D. D. Click Modification of a Metal-Organic Framework for Two-Photon Photodynamic Therapy with Near-Infrared Excitation. *ACS Appl. Mater. Interfaces*, **2021**, 13, 9739-9747.

[7] Collin J. P., Dixon I. M., Sauvage J. P., Williams J. A. G., Barigelletti F. and Flamigni L. Synthesis and Photophysical Properties of Iridium(III) Bisterpyridine and Its Homologues: a Family of Complexes with a Long-Lived Excited State. *J. Am. Chem. Soc.*, **1999**, 121, 5009-5016.

[8] P Nielsen., Toftlund H., Bond A. D., Boas J. F., Pilbrow J. R., Hanson G. R., Noble C., Riley M. J., Neville S. M., Moubaraki B. and Murray K. S. Systematic Study of Spin Crossover and Structure in $[Co(terpyRX)_2](Y)_2$ Systems (terpyRX = 4'-alkoxy-2,2':6',2''-terpyridine, X = 4, 8, 12, Y = BF_4^-, ClO_4^-, PF_6^-, BPh_4^-). *Inorg. Chem.*, **2009**, 48, 7033-7047.

[9] J. Zhao, K. W. Yan, G. Xu, X. Liu, Q. Zhao, C. J. Xu and S. H. Gou. An Iridium (III) Complex Bearing a Donor-Acceptor-Donor Type Ligand for NIR-Triggered Dual Phototherapy. *Adv. Funct. Mater.*, **2021**, 31, 2008325.

[10] C. K. Zhang, Y. Q. Zhao, D. D. Li, J. J. Liu, H. G. Han, D. Y. He, X. H. Tian, S. L. Li, J. Y. Wu and Y. P. Tian. Aggregation-induced emission (AIE)-active molecules bearing singlet oxygen generation activities: the tunable singlet-triplet energy gap matters. *Chem. Commun.*, **2019**, 55, 1450.

[11] B. Ni, H. Z. Cao, C. K. Zhang, S. L. Li, Q. Zhang, X. H. Tian, D. D. Li, J. Y. Wu and Y. P. Tian. Activated Type I and Type II Process for Two-Photon Promoted ROS Generation: The Coordinated Zn Matters. *Inorg. Chem.*, **2020**, 59, 13671-13678.